View metadata, citation and similar papers at core.ac.uk
brought to you by CORE
provided by Digital.CSIC

Film quality and electronic properties of a surface-anchored metal-organic framework as revealed by a multi-technique approach

Jianxi Liu,[a] Markos Paradinas,[b,c] Lars Heinke,[a] Manfred Buck,[c] Carmen Ocal,[b] Veronica Mugnaini,*[a,e] Christof Wöll*[a]

[a] Institute of Functional Interfaces (IFG), Karlsruhe Institute of Technology (KIT), 76344 Eggenstein-Leopoldshafen (Germany)
[b] Institut de Ci_ncia de Materials de Barcelona (ICMAB-CSIC), Campus de la UAB, 08193, Bellaterra (Spain)
[c] Catalan Institute of Nanoscience and Nanotechnology (ICN2) and the Barcelona Institute of Science and Technology
Campus de la UAB, 08193, Bellaterra (Spain)
[d] EaStCHEM School of Chemistry, University of St Andrews, North Haugh, St. Andrews KY16 9ST (UK)
[e] International Iberian Nanotechnology

*E-mail: veronica.mugnaini@inl.int

The virtually unlimited versatility and unparalleled level of control in the design of metal-organic frameworks (MOFs) has recently been shown to also carry a potential for applications based on the electrical and electronic properties of this rich class of materials. Since at present methods to provide reliable and reproducible contacts to MOF-materials are scarce, we have carried out a detailed, multi-technique investigation of an empty and loaded prototype MOF, HKUST-1. Epitaxial thin films of this material grown on a substrate using liquid-phase epitaxy have been studied by cyclic voltammetry (CV), atomic force microscopy (AFM), and quartz crystal microbalance (QCM), and their quality assessed. By using an ionic liquid (IL) as electrolyte it is shown that redox active molecules like ferrocene can be embedded in the pores, enabling to change the overall conductivity of the framework and to study the redox-chemistry of guest molecules inside the MOF.

Porous metal-organic frameworks (MOFs), also referred to as porous coordination polymers (PCP), are crystalline hybrid materials formed by metal nodes and organic linkers held together by coordination bonds.[1] The possibility to tailor their functionality either by the rational design of the organic ligands[2] or by filling the framework's pores with functional nano-objects[3] provides the basis for the continuously widening field of applications of MOFs,[4] with electronics[5] and batteries[6] as rather recent extensions. Using electroactive molecules[7] as linkers between the metal nodes or by doping the nanopores with electroactive guests,[3a,8] MOFs are indeed extremely appealing materials for electronics and implementation in so-called *MOFtronic* devices.[9] Although a huge potential is seen for MOFs in the field of electronics and also photovoltaics[10] the prediction and understanding of the electronic and electric properties are still in their incipiency due to the very limited number of studies reported so far.[11] A major reason, which is also a bottleneck for the actual integration of MOFs into a device, is represented by the fabrication of supported MOF thin films exhibiting the reproducible quality as regards their intrinsic properties like conductivity and the diffusion constant governing the loading with host molecules.[12]

Several strategies have been developed for fabricating MOFs as thin films.[13] Among these, the liquid phase epitaxy (LPE)[13a,e-h] appears as one of the most appropriate preparation methods to meet the requirements for electronic applications of MOFs. Through a stepwise growth of the MOF on a self-assembled monolayer (SAM) whose chemical functionality and/or packing density can be tailored at will,[14] continuous crystalline layers on a surface are obtained, referred to as SURMOFs (surface- anchored metal-organic framework). The functionalization of the supporting substrate, the choice of the growth method and the number of growth cycles allows for a precise control over the film thickness and the crystallographic orientation of the

MOF thin film.[13a] In addition, the LPE process allows the fabrication of hetero-multilayers in a straightforward fashion.[15] For the device applications of MOFs, the following topics are of paramount interest: firstly, the preparation of robustly surface-anchored and defect-free thin films covering extended areas on the order of cm^2; secondly, the identification of the most suitable techniques to characterize and monitor them. Indeed, the most widely used SURMOF characterization techniques (X-ray diffraction, XRD, and infrared reflection absorption spectroscopy, IRRAS) allow only for the determination of the long-range crystalline order of MOF thin films and their chemical composition, respectively. However these methods are not very sensitive to the presence of pinholes and other structural defects that could unpredictably alter the electrical properties of the SURMOF film when attaching a top electrode. Imaging techniques, such as atomic force microscopy (AFM), allows the observation of the surface, the determination of the film roughness and, eventually, the presence of defects, but only within a small (μm^2) area. [16] To gain insight into defect densities on a mm^2 or even cm^2 area AFM measurements alone become extremely time-consuming.

Herein we will present cyclic voltammetry (CV), in combination with AFM, as a fast method to determine the quality of SURMOF films used as working electrodes in a home-made electrochemical cell with platinum wires as counter and reference electrodes (see Figure S1 in Supporting Information (SI)). Eventually, we will also show the suitability of cyclic voltammetry as characterization technique for SURMOF films loaded with a small electroactive molecule, ferrocene, and demonstrate how important information on the conduction mechanism can be deduced from the shape of the cyclic voltammogram.

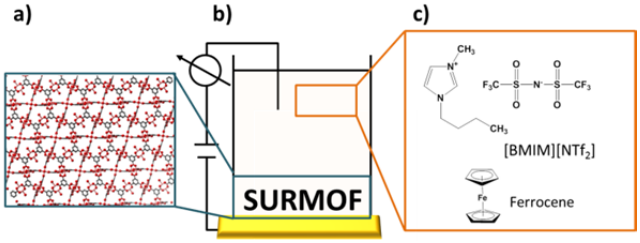

Figure 1. Schematic representation of the use of SURMOF as working electrodes in an electrochemical cell. a) Side view of HKUST-1 crystal structure grown along the [111] direction on a CMMT SAM. In red, oxygen; in blue, copper; in black, carbon. b) Schematic representation of the electrochemical cell. c) Molecular formula of the used ionic liquid (IL) and of ferrocene.

We have investigated the surface-anchored porous and crystalline HKUST-1 (also called $Cu_3(BTC)_2$, where BTC is *1,3,5*-benzenetricarboxylic acid)[17] grown by LPE on a gold electrode modified with a SAM.

In going beyond previous work reported by some of us[8a] we have studied different types of SAMs to initiate the MOF-growth. More specifically, CMMT (9-carboxy-10-(mercaptomethyl)triptycine, SAM1), and TPMTA (4'-carboxyterphenyl-4-methanethiol, SAM2) were chosen to functionalize the supporting Au-substrate. In both cases crystalline and oriented films (herein named SAM1/MOF, and SAM2/MOF, respectively) of different crystallographic orientation were obtained.[14] Figure 1a shows the case of SAM1/MOF HKUST-1 crystalline films with the [111] direction parallel to the surface normal.

The electrochemical measurements were carried out in an aprotic ionic liquid (IL), 1-butyl-3-methylimidazolinium bis(trifluoronethylsulfonyl)-imide, [BMIM][NTf_2] (Figure 1c), acting as solvent and supporting electrolyte. The ionic components of this IL do not interfere with the coordination bonds in the HKUST-1 SURMOF and preserve it from losing its crystalline structure (see Figure S2 in SI). Moreover, as several other known ionic liquids,[18] the used [BMIM][NTf_2] is a good supporting electrolyte for *a)* its electrochemical inertness (*i.e*. its wide potential window, larger than the one of the electroactive species under study) and *b)* its high conductivity.

Of course, the supporting electrolyte in the specific case of a cyclic voltammetry experiment has to be able to penetrate and diffuse in the pores of the SURMOF HKUST-1. Due to the rather small size of the [BMIM][NTf_2], it is reasonable to assume that it will diffuse inside the pores of the SURMOF. Nevertheless, since this is a crucial point, we used a quartz crystal microbalance (QCM)[12, 19] to determine the total uptake of the ionic liquid.

In a QCM experiment, the changes in resonance frequency of an oscillating sensor crystal are monitored in real time. Thanks to the relationship between resonance frequency shift and adsorbed/trapped mass, information on the amount of material deposited on sensor can be calculated.

A straightforward experiment to investigate the uptake of a guest molecule by a SURMOF-coated QCM sensor consists of letting a solvent (such as ethanol) flow over the QCM sensor and then exchanging it with the solution of the guest molecule whose uptake by the SURMOFs is to be studied (ferrocene in IL, in the specific case). In the case of IL, however, this is not feasible in the way described above: changes in frequency measured by QCM are very sensitive to variations in the viscosity[20] and the IL used has a much higher viscosity and density[18, 21] than the ethanol. Indeed, when the sample was exposed to the IL solution, the mass changes recorded by the QCM could not be unambiguously ascribed to the IL uptake.

Therefore, in order to investigate whether there is an IL uptake by the HKUST-1 SURMOF, we proceeded as follows: first, the sample was activated under argon gas flow at 60° for at least 6 hours. Then, pure liquid ethanol (EtOH) was flowed through the activated SURMOF HKUST-1 (Figure 2, red part). After 150 minutes, the surface was exposed to the IL/EtOH (96:4, volume ratio) solution. When the solvent was exchanged from EtOH to IL/EtOH (Figure 2, green part), an increase of the SURMOF mass of 22 µg/cm2 was calculated using the Sauerbrey equation,[22] which is a hint that IL diffuses into the SURMOF. It is important to stress, that the Sauerbrey equation is only correct under the assumption of a thin film approximated as rigid and for which the energy dissipation can be neglected. In the experiments here presented, however, by moving from gas to liquid phase (and vice versa) we significantly change the viscosity of the environment in contact with the sensing crystal, and hence we record a rather high dissipation change (data not shown). This means the determined values of mass changes (Fig. 2), calculated from the frequency changes, serve only as rough estimation of mass uptake.

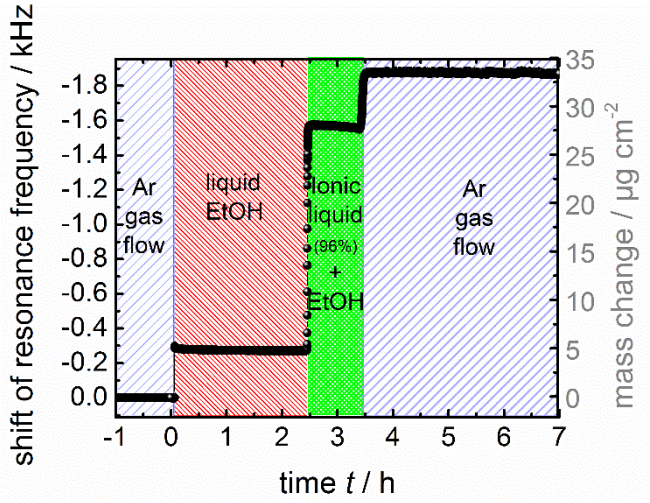

Figure 2. Ionic liquid uptake by HKUST-1 SURMOF measured by QCM. The shift in resonance frequency is plotted on the left y-axis, while the corresponding calculated mass change, estimated by the Sauerbrey equation, is plotted on the right y-axis.

When the argon is switched on, we experimentally observe a small change in frequency that corresponds to a calculated mass increase of about 4 µg cm^{-2}. A possible reason for the change in the resonance frequency and hence the associated mass increase is the following, according to the authors' opinion: as soon as the argon is switched on, EtOH molecules forming the IL:EtOH mixture evaporate, while the IL does not due to its low vapor pressure. This results in an increased IL-ratio and an increased density of the mixture inside the QCM-cell (and then in the SURMOF). The density and viscosity of IL, higher than the ones of its ethanolic mixture, is believed to be responsible for the mass increase.

A further experiment to prove that the IL can be loaded into the pores of the SURMOFs is shown in Figure S3. In this case the sample, which was loaded with IL and subsequently activated at 60° in an argon flow, was exposed to pure EtOH for 10 min and then again activated in an argon flow. In this case, the significant decrease in mass caused by the purging with EtOH indicates that, during this EtOH rinsing step, the IL leaves the SURMOF pores and is substituted by EtOH. By activation, the EtOH-filled pores are emptied.

We conclude, based on these QCM experiments, that the SURMOF can be loaded with the IL and hence that this is a suitable solvent/supporting electrolyte system.

HKUST-1 SURMOFs produced on both CMMT and TPMTA SAMs modified gold substrate were prepared by means of the spray method[23] and characterized by IRRAS and XRD (Figures S4 and S5).

Thereafter, the SURMOF HKUST-1 films were characterised by cyclic voltammetry employing ferrocene (Fc, see Figure 1c), an electroactive molecule less than 3.4 Å in size and widely used as standard in electrochemical investigations.[24] Using a 5 mM solution in IL/EtOH (96/4, v/v) the CVs of SURMOF HKUST-1 on either SAM1 (Figure 3a, in black) or SAM2 (Figure 3b, in black) were recorded in the range between -0.35 V and +0.55 V (*vs* Pt). Interestingly, the CVs are rather flat and, in particular, lack any features characteristic for the ferrocene/ferrocenium redox couple. This observation reveals that under the conditions and time frame of this experiment the redox active Fc species present in the solution do not reach the metal substrate to a significant extent. Combining the results from cyclic voltammetry with the ones from QCM, we conclude that the ionic liquid diffuses into the pores of the SURMOFs and, in combination with the confined space of the framework pores, essentially prevents the Fc molecules from moving across the HKUST-1 layer. We would like to note at this point that the CVs do not exhibit any features characteristic of the presence of defects acting as micro/nanoelectrodes[25] which indicates that the SURMOF layer is homogeneous and free of substantial defects such as pinholes. How the presence of defects alters the CV is demonstrated by a sample which has been intentionally damaged by simply scratching across the sample (see Figure S6). The pronounced change in the diffusion properties is reflected by the transition from the flat CV of the pristine SURMOF layer towards the sigmoidal shape of a microelectrode,[25] even though its shape is distorted as the scratch produces an ill-defined break-up of the SURMOF layer.

A completely different scenario occurs if the HKUST-1 SURMOF is loaded with ferrocene from the vapor phase[8a, 26] after activation of the MOF by soft annealing. The successful loading was proved by XRD and IRRAS. Showing the vibrational fingerprint of ferrocene the latter testifies the loading of the MOF with ferrocene (Figure S4). In the XRD 2□ scan (Figure S5), the decrease in the ratio of the (222) and (333) reflections is caused by the iron of the ferrocene, that is a quite strong X-ray scatterer. This also indicates the presence of the molecule in the framework pores. However, even more important is that the crystallinity is not adversely affected by the ferrocene uptake, this being crucial for the interpretation of the electrochemical data.

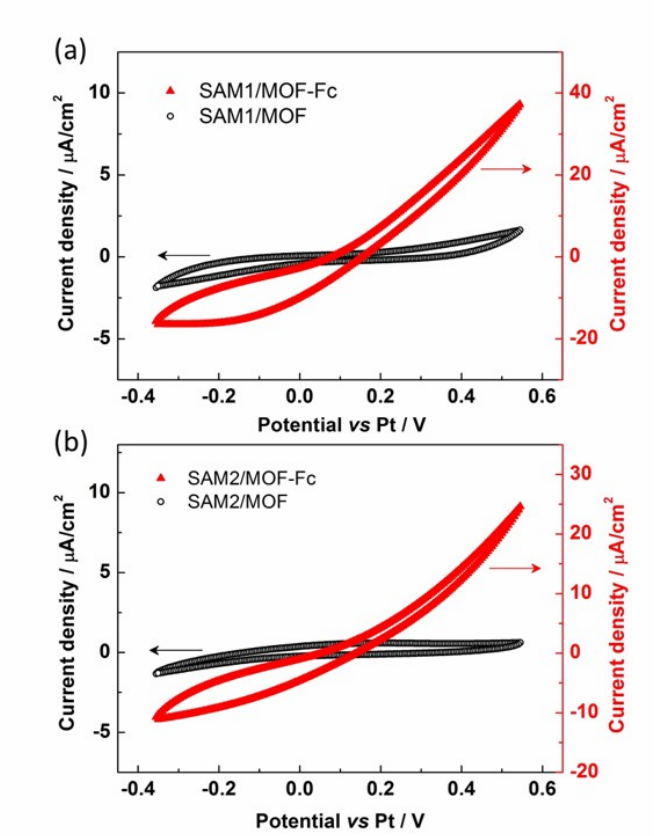

Figure 3. (a) CV of SAM1/MOF (black) and SAM1/MOF-Fc (red) recorded at a scan rate of 20 mV/s. (b) (b) CV of SAM1/MOF (black) and SAM1/MOF-Fc (red) recorded at a scan rate of 20 mV/s.

The cyclic voltammograms (red curves in Figure 3) are pronouncedly different from the unmodified MOF as they now exhibit a quasi-linear increase in current density in the measured voltage range up to a value of 40 □A/cm2 at +0.55 V at a scan rate of 20 mV/s for SAM1/MOF-Fc and analogously for SAM2/MOF. In principle, the difference in the CVs of the Fc loaded and unloaded SURMOF layers can be explained by two mechanisms. In

one case the Fc/Fc+ redox reaction takes place at the MOF-metal interface and the current is mass transport limited due to a strongly hindered diffusion of Fc in the MOF compared to the bulk ionic liquid which would give rise to a grossly distorted CV. The other interpretation is a charge-hopping mechanism where the Fc molecules remain localised in the pores of the MOF and mediate the electron transport across the layer. In this case the Fc/Fc+ redox reaction takes place at the MOF-IL interface. Given that the IL loaded MOF is impermeable for Fc as demonstrated above and the crystallinity of the Fc loaded MOF is not differing from the unloaded one, the first mechanism, which has been observed for post-synthetically modified surface anchored gels,[27] is excluded. Furthermore, the essentially identical current density vs voltage dependencies at different scan rates (Figure S7) contradicts a diffusion process. Since an analogous charge-hopping mechanism was also reported for HKUST-1 grown along the [001] direction on mercaptohexadecanoic acid (MHDA) SAM,[8a] the present finding demonstrates that this is a general property of this MOF structure as it is not independent on the SURMOF crystallographic orientation.

Looking at the CVs of the Fc loaded MOFs (Figures 3, S7) and the mechanically damaged one (Figure S6) there is a significant cathodic current in the reverse scan direction which indicates that diffusion of Fc+ away from the MOF surface is incomplete. While the reasons for this are not established yet we tentatively explain this with the topography of the outer surface of the MOF which, as revealed by AFM (Figures S9/10), exhibits a significant roughness and graininess. Nanoscopic kinks, pockets and grooves in the near surface region would, therefore, cause deviations from a free diffusion. Differences in the surface morphology could also account for small differences between the CVs.

A closer look at the quasi-linear plot of the current density vs voltage shows two regimes differing in slope: In the anodic range (from +0.14V to +0.55V) a resistance of 45.5 kΩ can be calculated for SAM1/MOF-Fc, and of 63 kΩ for SAM2/MOF-Fc (from the current density vs voltage dependence at a scan rate of 20 mV/s, Table 1). In the cathodic range (from -0.35V to +0.14V), where the linearity of the current density vs voltage is less pronounced, a resistance of 236 kΩ for SAM1/MOF-Fc, and 224 kΩ for SAM2/MOF-Fc can be calculated (Table 1). This means that ferrocenium cations (formed in the anodic region and known to have a larger conductivity than neutral ferrocene)[24b] are indeed generated inside the pores as result of the charge hopping taking place inside the framework.[28]

Table 1. Anodic and cathodic resistance and conductivity for SAM1/MOF-Fc and SAM2/MOF-Fc. As thickness, values of 70 ± 5 nm for SAM1/MOF-Fc and 75 ± 5 nm for SAM2/MOF-Fc have been used.

	Anodic Range: from 0.14V to 0.55V		**Cathodic Range: from -0.35V to -0.14V**	
	R / kΩ	**σ_a / S·cm^{-1}**	**R / kΩ**	**σ_c / S·cm^{-1}**
SAM1/MOF-Fc	45.5	$5.1 \pm 0.3 \times 10^{-10}$	236	$9.9 \pm 0.15 \times 10^{-11}$
SAM2/MOF-Fc	63	$4.0 \pm 0.3 \times 10^{-10}$	224	$1.1 \pm 0.05 \times 10^{-10}$

The conductivity of SURMOFs HKUST-1 was calculated from the resistance values after measuring the sample thickness by atomic force microscopy, as presented in Figure 4. The topographic images show orientated crystallites of HKUST-1, likely as result of the LPE method chosen for the sample preparation. Nevertheless, these crystallites are sitting on top of a continuous and rather homogeneous MOF layer (see bottom right regions in Fig 4c and 4d and explanation of film scratching in the experimental section), confirming the presence of a defect free film as inferred from cyclic voltammetry experiments.

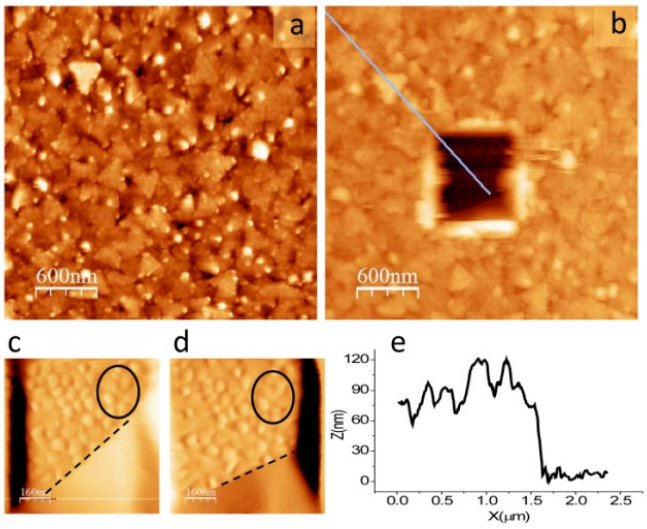

Figure 4. Topographic AFM images before (a) and after (b) local removal of the SURMOF on sample SAM1/MOF (imaging force ~10 nN). Selected images (c and d) taken during the scratching (□500 nN load). Ellipses in (c) and (d) indicate the same areas of cleared substrate gold grains (800 nm x 800 nm). Dashed lines indicate removal front (for details see text and SI). The relief profile in (e) is along the line in (b) and illustrates the surface roughness and thickness of the SURMOF.

The average vertical dimension of the crystallites is ~20 nm and ~35 nm for SAM1/MOF-Fc and SAM2/MOF-Fc, respectively, whereas the underlying HKUST-1-Fc films exhibits a thickness of □70 ± 5 nm for SAM1/MOF-Fc (see profile in Figure 4e) and ~75 ± 5 nm for SAM2/MOF-Fc (Figure S11). Using the thickness of the homogeneous SURMOF layer as determined by AFM and the electrochemical cell area, the calculated conductivity values (σ) at room temperature for each range result in σ_a = 5.1 ± 0.3 × 10-10 S·cm-1 and in σ_c = 9.9 ± 0.15 × 10-11 S·cm-1 for the anodic and cathodic ranges for SAM1/MOF-Fc, respectively (Table 1). The corresponding values for SAM2/MOF-Fc are σ_a = 4.0 ± 0.3 × 10-10 S·cm-1 and σ_c = 1.1 ± 0.05 × 10-10 S·cm-1 (Table 1). These conductivities are somewhat lower than the ones provided in our previous report.[8a] These differences are attributed to variations in sample quality. Note that these conductivity values are a lower limit as only the homogenous and continuous HKUST-1 layers are considered. Indeed, contributions from the on top grown crystallites can also be considered. For the sake of simplicity, we take into account only the mean vertical size of the crystallites (~20 nm and ~35 nm for SAM1/MOF and SAM2/MOF, respectively) and not their contribution to the increase in surface area: by doing that an upper value of conductivity σ_a = 6.6 × 10-10 S·cm-1 and σ_a = 5.8 × 10-10 S·cm-1, respectively, is obtained. These values are in good agreement with electric conductivity values measured for the SAM1/MOF-Fc films upon their integration in a Hg-based tunneling junction[29].

In conclusion, we have demonstrated that the spray based LPE method is suitable to produce crystalline and defect free films of HKUST-1 on different SAMs and that the film quality is independent on crystallographic orientation of the film. In combination with other characterisation techniques, it is shown that by means of cyclic voltammetry the presence of defects or pinholes can be determined for SURMOFs covering macroscopic areas in a fast and straightforward fashion. Additionally, by means of cyclic voltammetry, we have also been able to gain further insight into the electronic properties of SURMOF HKUST-1 loaded with ferrocene. When ferrocene molecules are embedded inside the HKUST-1 pores, they are involved in a charge hopping mechanism that leads to a reversible ferrocene-ferrocenium redox process that takes place along the pores-immobilized guests and eventually triggers the oxidation of ferrocene electrolyte at the IL/MOF interface.

Following the presented strategy, electrochemical characterization of other SURMOFs with ferrocene and other electroactive molecules is in progress and will help us to shed light on the relation between SURMOF crystalline orientation and pore size, morphology and lateral homogeneity, and their electrochemical behaviour. In addition, we plan to carry out further experiments to elucidate the role of the used supporting electrolyte as well as of the electroactive guests immobilised in the SURMOF.

Experimental Section

SAM Preparation

SAMs were formed on gold substrates (100 nm of Au on Si substrate, with a 5 nm Ti adhesion layer; purchased from Georg Albert PVD) or on QCM sensors (Au coated, purchased from LOT-ORIEL) by immersion into solutions of CMMT (9-carboxy-10-(mercaptomethyl) triptycene) and TPMTA (4'-carboxyterphenyl-4-methanethiol), as described in the literature.[14]

Preparation of SURMOF HKUST-1 and characterization by means of out-of-plane XRD and IRRAS

The HKUST-1 SURMOFs on CMMT and TPMTA, SAM1/MOF and SAM2/MOF, respectively, were prepared in a stepwise fashion using the spray method (copper acetate mono-hydrate, 1 mM in ethanol; 1,3,5-benzenetricarboxylic acid, 0.1 mM in ethanol; both purchased from Sigma Aldrich and used without further purification). This method[23] is a modification of the well described LPE[13g] method that drastically reduces the time needed for sample preparation, without affecting neither the crystallinity nor the definition of the crystallographic orientation. Indeed, out-of-plane XRD (Bruker D8-Advance diffractometer) patterns show a good crystallographic orientation for SAM1/MOF (Figure S5a) and a less pronounced orientation for SAM2/MOF (Figure S5b). The loading with ferrocene (Fc, from Sigma Aldrich and used without further purification) was done by exposure of SAM1/MOF and SAM2/MOF to Fc vapours in a sealed vial[8a] for a time of typically 64 h after activation of the samples (20 minutes at 60 °C) in a vacuum oven which removes residual solvent molecules trapped in the pores. The resulting Fc loaded samples, named herein SAM1/MOF-Fc and SAM2/MOF-Fc respectively, were characterized by IRRAS and out-of-plane XRD (Figures S4 and S5, in red).

Quartz Crystal Microbalance

A quartz crystal microbalance (QCM, of type E4 from Q-Sense) was used for quantifying the IL uptake by the SURMOF. The solutions were pumped at a flow rate of 0.5 ml/min through the QCM cell; the argon flow rate was 100 ml/min. The loading experiments as well as the activation in argon were performed at a temperature of 60°C.

Electrochemical measurements

Cyclic voltammetry (CV) was carried out in a home-built electrochemical cell using a standard three electrode set-up, with reference (placed in a Luggin capillary) and counter electrodes made from platinum wires (diameter 0.25 mm, Advent Research Materials Ltd). The area of the working electrode was 0.3 cm2. Measurements of SAM1, SAM1/MOF, SAM1/MOF-Fc, SAM2, SAM2/MOF, SAM2/MOF-Fc were done under continuous argon flow. A PalmSens potentiostat was used. As supporting electrolyte, the aprotic ionic liquid (IL) 1-butyl-3-methylimidazolinium bis(trifluoronethylsulfonyl)-imide ([BMIM][NTf2]) from io-li-tec, (structure presented in Figure 1(c)), was chosen and ferrocene (5 mM) was dissolved by adding a small amount of ethanol (4/96 EtOH/[BMIM][NTf2]). CVs were acquired by exposing the sample to the solution of ferrocene (Figure 1c) in [BMIM][NTf2]. The potential window was kept constant for all the experiments (from -0.35 to +0.55 V vs Pt) while the scan rate was varied (20 mV/s, 50 mV/s, 100 mV/s). After the electrochemical experiments the samples were routinely checked by XRD, and no loss in in the crystalline structure of the SURMOF could be observed (see Figure S2).

Atomic force microscopy measurements

As done previously for similar systems, the thickness of the samples after ferrocene loading was accurately determined by atomic force microscopy (AFM) employing the scratching method.[16b] The AFM images (Figure 4 and Figure S10) clearly show on both template surfaces SAM1 and SAM2 the presence of oriented crystallites of HKUST-1. As seen in Figure 4a for SAM1/MOF-Fc, though randomly distributed in azimuth, the crystallites exhibit a flat top surface with a clear triangular shape indicative of a (111) orientation, in agreement with the XRD data shown in Figure S5. Details of the morphology and orientation of the crystallites for SAM2/MOF are shown in Figure S10. Scratching experiments (details in SI) were performed on the very same surface region (see Figure 4b) to remove the grown MOF until the underlying gold substrate is completely uncovered (Figure 4, and Figures S10-S11). Figure 4c and 4d correspond to images taken at the central part of the region in 4b during the scratching and serve to illustrate the process. The small grains of the underlying gold substrate are clearly recognized in the cleared areas. To be used as a reference, the same gold grains have been circled in both images and a dashed line has been drawn in each image to mark the material removal front. Note the movement of the front between 4c and 4d. The AFM measurements were performed under low humidity conditions (<5 % RH, obtained by a continuous N2 flux) using a commercial head and electronics from Nanotec.[30] Si probes from Nanosensors with an intermediate spring constant (k = 2.8 N/m) were used. The imaging force was set to below 10 nN while a force in the range of 400-700 nN was applied to remove the MOF (see SI for more details).

Acknowledgements

VM acknowledges the EU for the funding through the granting of a Marie Curie Intra-European Fellowship (FP7-PEOPLE-2011; MOLSURMOF-301110). JL acknowledges the program of China Scholarship Council (CSC) for financial support. VM, JL and CW acknowledge A. Terfort for supplying the thiol derivatives. MP and CO acknowledge financial support from the Spanish Government through grants projects MAT2013-47869-C4-1-P and SEV-2015–0496, and Generalitat de Catalunya through grant project 2014 SGR 501. VM and JL thank P.G. Weidler for the useful help in the analysis of XRD data.

REFERENCES

[1] a) S. I. Noro, S. Kitagawa, in The Supramolecular Chemistry of Organic-Inorganic Hybrid Materials, ed. K. Rurack and R. Martínez-Máñez, John Wiley & Sons, Inc. 2010, pp. 235–269; b) S. L. James, Chem. Soc. Rev. 2003, 32, 276-288.

[2] a) H. Furukawa, N. Ko, Y. B. Go, N. Aratani, S. B. Choi, E. Choi, A. O. Yazaydin, R. Q. Snurr, M. O'Keeffe, J. Kim, O. M. Yaghi, Science 2010, 329, 424-428; b) D. Zhao, D. J. Timmons, D. Q. Yuan, H. C. Zhou, Acc. Chem. Res. 2011, 44, 123-133; c) F. A. A. Paz, J. Klinowski, S. M. F. Vilela, J. P. C. Tome, J. A. S. Cavaleiro, J. Rocha, Chem. Soc. Rev. 2012, 41, 1088-1110.

[3] a) P. R. McGonigal, P. Deria, I. Hod, P. Z. Moghadam, A-J Avestro, N. E. Horwitz, I. C. Gibbs-Hall, A. K. Blackburn, D. Chen, Y. Y. Botros, M. R. Wasielewski, R. Q. Snurr, J. T. Hupp, O. K. Farha, J. F. Stoddart, PNAS. 2015, 112, 11161-11168; b) B. Liu, H. Shioyama, T. Akita, Q. Xu, J. Am. Chem. Soc. 2008, 130, 5390-5391; c) M. Meilikhov, K. Yusenko, A. Torrisi, B. Jee, C. Mellot-Draznieks, A. Poppl, R. A. Fischer, Angew. Chem., Int. Ed. 2010, 49, 6212-6215.

[4] P. Falcaro, R. Ricco, C. M. Doherty, K. Liang, A. J. Hill, M. J. Styles, Chem. Soc. Rev. 2014, 43, 5513-5560.

[5] a) M. Usman, S. Mendiratta, K-L. Lu, ChemElectroChem. 2015, 2, 786-788; b) A. Morozan, F. Jaouen, Energy Environ. Sci. 2012, 5, 9269-9290; c) M. D. Allendorf, A. Schwartzberg, V. Stavila, A. A. Talin, Chem. Eur. J. 2011, 17, 11372-11388.

[6] a) Z. Y. Zhang, H. Yoshikawa, K. Awaga, J. Am. Chem. Soc. 2014, 136, 16112-16115; b) D. F. Wu, Z. Y. Guo, X. B. Yin, Q. Q. Pang, B. B. Tu, L. J. Zhang, Y. G. Wang, Q. W. Li, Adv. Mater. 2014, 26, 3258-3262.

[7] a) S. Takaishi, M. Hosoda, T. Kajiwara, H. Miyasaka, M. Yamashita, Y. Nakanishi, Y. Kitagawa, K. Yamaguchi, A. Kobayashi, H. Kitagawa, Inorg. Chem. 2009, 48, 9048-9050; b) Y. Kobayashi, B. Jacobs, M. D. Allendorf, J. R. Long, Chem. Mater. 2010, 22, 4120-4122; c) K. Hirai, H. Uehara, S. Kitagawa, S. Furukawa, Dalton Trans. 2012, 41, 3924-3927; d) T. C. Narayan, T. Miyakai, S. Seki, M. Dinca, J. Am. Chem. Soc. 2012, 134, 12932-12935; e) D. Umeyama, S. Horike, M. Inukai, T. Itakura, S. Kitagawa, J. Am. Chem. Soc. 2012, 134, 12780-12785.

[8] a) A. Dragasser, O. Shekhah, O. Zybaylo, C. Shen, M. Buck, C. Wöll, D. Schlettwein, Chem. Commun. 2012, 48, 663-665; b) A. A. Talin, A. Centrone, A. C. Ford, M. E. Foster, V. Stavila, P. Haney, R. A. Kinney, V. Szalai, F. El Gabaly, H. P. Yoon, F. Leonard, M. D. Allendorf, Science 2014, 343, 66-69.

[9] V. Stavila, A. A. Talin, M. D. Allendorf, Chem. Soc. Rev. 2014, 43, 5994-6010.

[10] J. Liu, W. Zhou, J. Liu, I. Howard, G. Kilibarda, S. Schlabach, D. Coupry, M. Addicoat, S. Yoneda, Y. Tsutsui, T. Sakurai, S. Seki, Z. Wang, P. Lindemann, E. Redel, T. Heine, C. Wöll, Angew. Chem., Int. Ed. 2015, 54, 7441-7445.

[11] a) C. H. Hendon, D. Tiana, A. Walsh, Phys. Chem. Chem. Phys. 2012, 14, 13120-13132; b) K. T. Butler, C. H. Hendon, A. Walsh, J. Am. Chem. Soc. 2014, 136, 2703-2706.

[12] a) W. Zhou, C. Wöll, L. Heinke, Materials, 2015, 8, 3767-3775; b) L. Heinke, Z. G. Gu, C. Wöll, Nat. Commun. 2014, 5:4462.

[13] a) J-L. Zhuang, A. Terfort, C. Wöll, Coord. Chem. Rev. 2016, 307, 391-424; b) L. Heinke, M. Tu, S. Wannapaiboon, R. A. Fischer, C. Wöll, Microporous Mesoporous Mater. 2015, 216, 200-215; c) H. Al-Kutubi, J. Gascon, E.J.R. Sudhölter, L. Rassaei, ChemElectroChem. 2015, 2, 462-474; d) C. R. Wade, M. Y. Li, M. Dinca, Angew. Chem., Int. Ed. 2013, 52, 13377-13381; e) N. Campagnol, T. Van Assche, T. Boudewijns, J. Denayer, K.

Binnemans, D. De Vos, J. Fransaer, J. Mater. Chem. A 2013, 1, 5827-5830; f) T. R. C. Van Assche, G. Desmet, R. Ameloot, D. E. De Vos, H. Terryn, J. F. M. Denayer, Microporous Mesoporous Mater. 2012, 158, 209-213; g) O. Shekhah, J. Liu, R. A. Fischer, C. Wöll, Chem. Soc. Rev. 2011, 40, 1081-1106; h) A. Schoedel, C. Scherb, T. Bein, Angew. Chem., Int. Ed. 2010, 49, 7225-7228; i) O. Shekhah, H. Wang, D. Zacher, R. A. Fischer, C. Wöll, Angew. Chem., Int. Ed. 2009, 48, 5038-5041; i) C. Scherb, A. Schodel, T. Bein, Angew. Chem., Int. Ed. 2008, 47, 5777-5779.

[14] J. X. Liu, O. Shekhah, X. Stammer, H. K. Arslan, B. Liu, B. Schupbach, A. Terfort, C. Wöll, Materials 2012, 5, 1581-1592.

[15] Z. Wang, J. Liu, B. Lukose, Z. Gu, P. G. Weidler, H. Gliemann, T. Heine, C. Wöll, Nano Lett. 2014, 14, 1526-1529.

[16] a) C. Munuera, O. Shekhah, H. Wang, C. Wöll, C. Ocal, Phys. Chem. Chem. Phys. 2008, 10, 7257-7261; b) O. Shekhah, H. Wang, M. Paradinas, C. Ocal, B. Schupbach, A. Terfort, D. Zacher, R. A. Fischer, C. Wöll, Nat. Mater. 2009, 8, 481-484.

[17] S. S. Y. Chui, S. M. F. Lo, J. P. H. Charmant, A. G. Orpen, I. D. Williams, Science 1999, 283, 1148-1150.

[18] R. D. Rogers, K. R. Seddon, Science 2003, 302, 792-793.

[19] L. Heinke, C. Wöll, Phys. Chem. Chem. Phys. 2013, 15, 9295-9299.

[20] I. Goubaidoulline, G. Vidrich, D. Johannsmann, Anal. Chem. 2005, 77, 615-619.

[21] a) S. J. Zhang, N. Sun, X. Z. He, X. M. Lu, X. P. Zhang, J. Phys. Chem. Ref. Data 2006, 35, 1475-1517; b) J. Jacquemin, P. Husson, A. A. H. Padua, V. Majer, Green Chem. 2006, 8, 172-180.

[22] G. Sauerbrey, Zeitschrift Fur Physik 1959, 155, 206-222.

[23] H. K. Arslan, O. Shekhah, J. Wohlgemuth, M. Franzreb, R. A. Fischer, C. Wöll, Adv. Funct. Mater. 2011, 21, 4228-4231.

[24] a) A. D. Le, L. Yu, J. Electrochem. Soc. 2011, 158, F10-F14; b) D. O. Cowan, Y. Sasaki, J. Park, C. U. Pittman, Mukherje.Tk, N. A. Diamond, J. Am. Chem. Soc. 1972, 94, 5110-5112.

[25] J. Heinze, Angew. Chemie Int. Ed. 1993, 32, 1268-1288.

[26] M. J. S. Monte, L. M. N. B. F. Santos, M. Fulem, J. M. S. Fonseca, C. A. D. Sousa, J. Chem. Eng. Data 2006, 51, 757-766.

[27] V. Mugnaini, M. Tsotsalas, F. Bebensee, S. Grosjean, A. Shahnas, S. Brase, J. Lahann, M. Buck, C. Wöll, Chem. Commun. 2014, 50, 11129-11131.

[28] Note: There is a typographical error in the unit of the resistance provided for the HKUST-1 SURMOF in ref. 8a. Instead of 31 MΩ it should read 31 kΩ. The conductivity values provided in this ref. are correct.

[29] J. Liu, T. Wachter, A. Irmler, P. G. Weidler, H. Gliemann, F. Pauly, V. Mugnaini, M. Zharnikov, C. Wöll, ACS Appl. Mater. Interfaces 2015, 7, 9824-9830.

[30] I. Horcas, R. Fernandez, J. M. Gomez-Rodriguez, J. Colchero, J. Gomez-Herrero, A. M. Baro, Rev. Sci. Instrum. 2007, 78:013705.